Optical Materials 60 (2016) 546–551

Contents lists available at ScienceDirect

Optical Materials

journal homepage: www.elsevier.com/locate/optmat

Thermal analysis of a diffusion bonded Er^{3+},Yb^{3+}:glass/Co^{2+}: $MgAl_2O_4$ microchip lasers

Nabil Belghachem*, Jaroslaw Mlynczak, krzysztof Kopczynski, Zygmunt Mierczyk, Michal Gawron

Institute of Optoelectronics, Military University of Technology, Kaliskiego 2 Str., 00-908 Warsaw, Poland

ARTICLE INFO

Article history:
Received 18 July 2016
Received in revised form
22 August 2016
Accepted 6 September 2016
Available online 15 September 2016

Keywords:
Microchip laser
Q-switched laser
Heat sink effect
Thermal expansion
Von mises stress
Diffusion bonding
Thermal focal length

ABSTRACT

The analysis of thermal effects in a diffusion bonded Er^{3+},Yb^{3+}:glass/Co^{2+}:$MgAl_2O_4$ microchip laser is presented. The analysis is performed for both wavelengths at 940 nm and at 975 nm as well as for two different sides of pumping, glass side and saturable absorber side. The heat sink effect of Co^{2+}:$MgAl_2O_4$, as well as the impact of the thermal expansion and induced stress on the diffusion bonding are emphasised. The best configurations for reducing the temperature peaks, the Von Mises stresses on the diffusion bonding, and the thermal lensing are determined.

1. Introduction

In the last years, diode end pumped erbium ytterbium glass microchip lasers have been widely used for different applications mostly due to their compactness, low cost and incredible efficiency. The simplicity of the passive q-switching using saturable absorbers like Co: MALO (Co^{2+}:$MgAl_2O_4$) allowed the generation of short nanosecond pulses with high peak power around the eye safe wavelength of 1.5 μm, perfect for telemetry applications [1–10].

Various researches were conducted in order to optimize the performances of such microchip lasers especially in the pulsed regime [12–15]. Recently, a compact 2.2 mm long microchip laser based on erbium ytterbium phosphate glass and Co:MALO saturable absorber was developed using the thermal diffusion bonding technology. The internal losses and size of the cavity were greatly reduced due to the diffusion bonding, thus the generation of short nanosecond pulses with 2.9 ns pulse duration and peak power up to 10 kW was possible [11].

Besides peak power and pulse duration, other important aspects should be studied: thermal effects and thermal lensing. Erbium ytterbium doped phosphate glasses are efficient for laser generation around 1.5 μm; nevertheless they have lower thermal conductivity than crystalline media. Moreover, the high absorption of the pump power, the quantum defects and the significant non-radiative transitions in the abundant energy level of Er^{3+} generate severe thermal effects. As a result, dramatic degradations occur in the output beam quality and power, this can even lead to the suppression of the laser generation. Also phosphate glasses have negative thermo-optical parameter and the stabilization of the microchip greatly depends on the thermo-mechanical effects.

In this paper, the study of the thermal effects and the thermal lensing in erbium-ytterbium phosphate glass diffusion bonded with Co:MALO saturable absorber is conducted. The analysis is based on numerically solving the heat equation and estimating the deformation of the end faces of the microchip laser as well as the Von Mises stresses. The best configurations for reducing the temperature peaks, the Von Mises stresses on the diffusion bonding and the thermal lensing are determined. According to the knowledge of the authors, no such analysis was done for such kind of microchip laser which could be very promising for compact and powerful pulsed microchip lasers.

* Corresponding author.
E-mail address: nabil.belghachem@wat.edu.pl (N. Belghachem).

http://dx.doi.org/10.1016/j.optmat.2016.09.021

2. Model and setup

The developed microchip laser is shown in Fig. 1. The phosphate glass named PAL is diffusion bonded with the Co:MALO saturable absorber (blue color). The concentration of the erbium and ytterbium are 8.9×10^{19} cm^{-3} and 1.94×10^{21} cm^{-3} respectively. The active media and the saturable absorber were polished to the thickness of 1.9 mm and 0.29 mm respectively. The input and output mirror were directly coated on the end faces (4×4 mm) of the microchip resulting in a 2.2 mm long plane parallel cavity. As pump source a 100 μm core diameter laser diode was used. The regime of pumping was quasi CW with 50% duty cycle and a period of 20 ms. The maximum average pump power used was 500 mW and no particular cooling system was used.

Various formulas were used in literature to describe the thermal effects and the thermal lensing [16–19] in a microchip laser. The well-known one was derived by Tidwell et al. [20]; however such formulas were derived basing on simplification assumptions which are not always true. These assumptions are related to the shape, the heat transfer direction, the deposited beam and the dimensions of the laser medium.

The thermal analysis of our microchip laser requires a more rigorous approach due to the diffusion bonding. Indeed, phosphate glass and MALO crystal have completely different material properties like heat conduction, thermal expansion and thermo-optical parameter. Furthermore, in this case the side of the pumping matters.

Thus, a rigorous approach consists of numerically solving the heat equation of the studied case using finite elements with no simplification assumptions. The general form of the heat equation can be described by:

$$\frac{1}{r}\frac{\partial}{\partial r}\left(r\frac{\partial T(r,\varphi,z,t)}{\partial r}\right)+\frac{1}{r^2}\frac{\partial^2 T(r,\varphi,z,t)}{\partial \varphi^2}+\frac{\partial^2 T(r,\varphi,z,t)}{\partial z^2}+\frac{Q(r,\varphi,z,t)}{K}=\frac{\rho c_p}{K}\frac{\partial T(r,\varphi,z,t)}{\partial t} \quad (1)$$

Where T is the temperature, K is the thermal conductivity and Q is the generated heat rate, ρc are the density and the specific heat, and r,φ,z are the cylindrical coordinates.

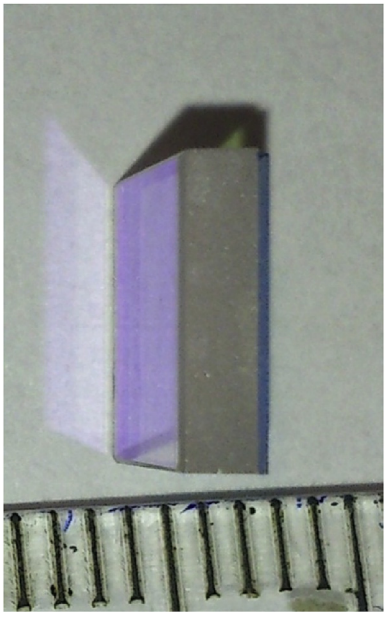

Fig. 1. Developed diffusion bonded Er:PAL/Co:MALO microchip laser.

The equation above is more general, the time dependence of $Q(r,\varphi,z,t)$ can be used to specify the CW or the pulsed pumping regime. In our case the frequency of pumping was 50 Hz which is much greater than the inverse of the thermal relaxation [21] (thermal time constant) which is given by:

$$\frac{1}{\tau_{th}}=\frac{4K}{c_p\rho r_b^2} \quad (2)$$

Where r_b is the center to edge distance of the microchip laser.

In this case the system is sensitive to the average input pump power and the steady state solution can be computed.

The heat equation was solved using finite elements with ultra-fine free tetrahedral mesh. The initial temperature of the microchip was equal to the ambient temperature in the lab 293.15 K. Concerning the boundary conditions the external faces of the microchip laser were subject to natural convection.

The simulation was done for both pumping wavelengths 940 nm and 975 nm which have different absorption cross-section. For each wavelength the Gaussian pumping radiation was incident on the front face (dichroic input mirror coated on the glass side) then on the back face (dichroic input mirror coated on the MALO crystal side) of the microchip, knowing that the back face refers to the side of the saturable absorber.

The parameters used for the simulation are detailed in Table 1. Once the heat equation is solved, the thermo-mechanical and optical effects can be estimated using multi-physics software taking into account the interaction between the glass and MALO crystal. Fig. 2 shows an exemplary solution.

3. Results and discussions

Fig. 3 shows the temperature distribution in a longitudinal cross-section of the microchip laser for each pumping case. The figure shows that in fact the temperature distribution varies for each wavelength and chosen pumping side. Indeed the high thermal conductivity of Co:MALO comparing to the glass ones makes that the Co:MALO acts like a heat sink which changes the temperature distribution.

One can see from Fig. 3 that the penetration of the 940 nm wavelength is higher than 975 nm, and in case of the front pumping the highest temperature is registered at the front face (pumped face) where the dichroic input mirror coating is located. When the average pump power is 500 mW, the highest temperature is 430 K at 975 nm. While at 940 nm it is much lower 335 K. In this configuration the most dangerous effects of the temperature rising

Table 1
Material parameters of phosphate glass and MALO crystal.

Parameters	Symbols [unit]	PAL	MALO
Thermal conductivity	K[W/mK]	0.745	7–15
Thermal expansion	α_T [1/K]	72×10^{-7}	80×10^{-7}
Temperature coefficient of the refractive index	dn/dT [1/K]	-27×10^{-7}	30×10^{-7}
Refractive index	n_{0glass}, n_{0MALO}	1.53	1.67
Poisson's ratio	υ	0.24	0.24
Density	ρ[kg/m^3]	2633	3500
Heat capacity at constant pressure	c_p[J/kgK]	840	290
Young's modulus	E [Pa]	70×10^9	2.3×10^5
Length	l_{glass},l_{MALO} [mm]	1.9	0.29
Absorption coefficient at 975 nm	α_0 [1/cm]	19.4	0.0783
Absorption coefficient at 940 nm	α_0 [1/cm]	4.28	0.0763
Quantum defects	ξ	0.3648	
Pump size radius	ω_p[μm]	50	

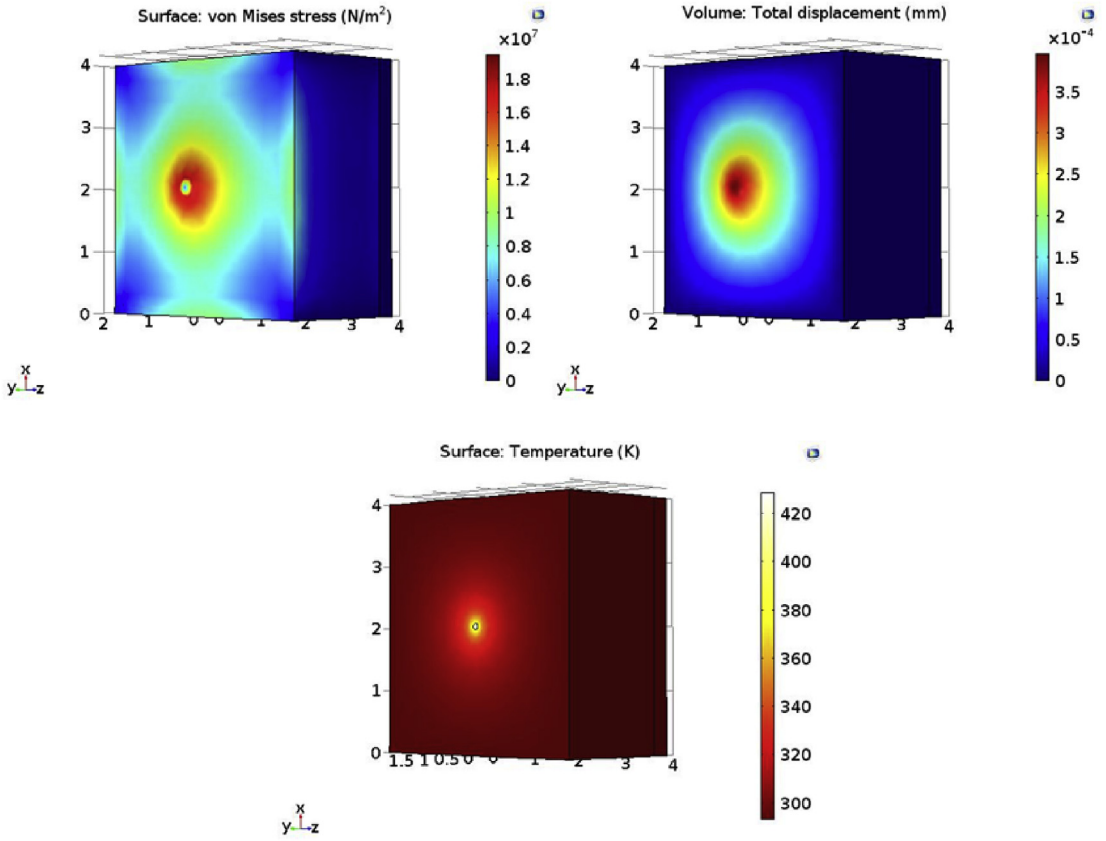

Fig. 2. Estimated Von Mises stress, displacement and temperature distribution in the case of 500 mW average power front pumping 975 nm.

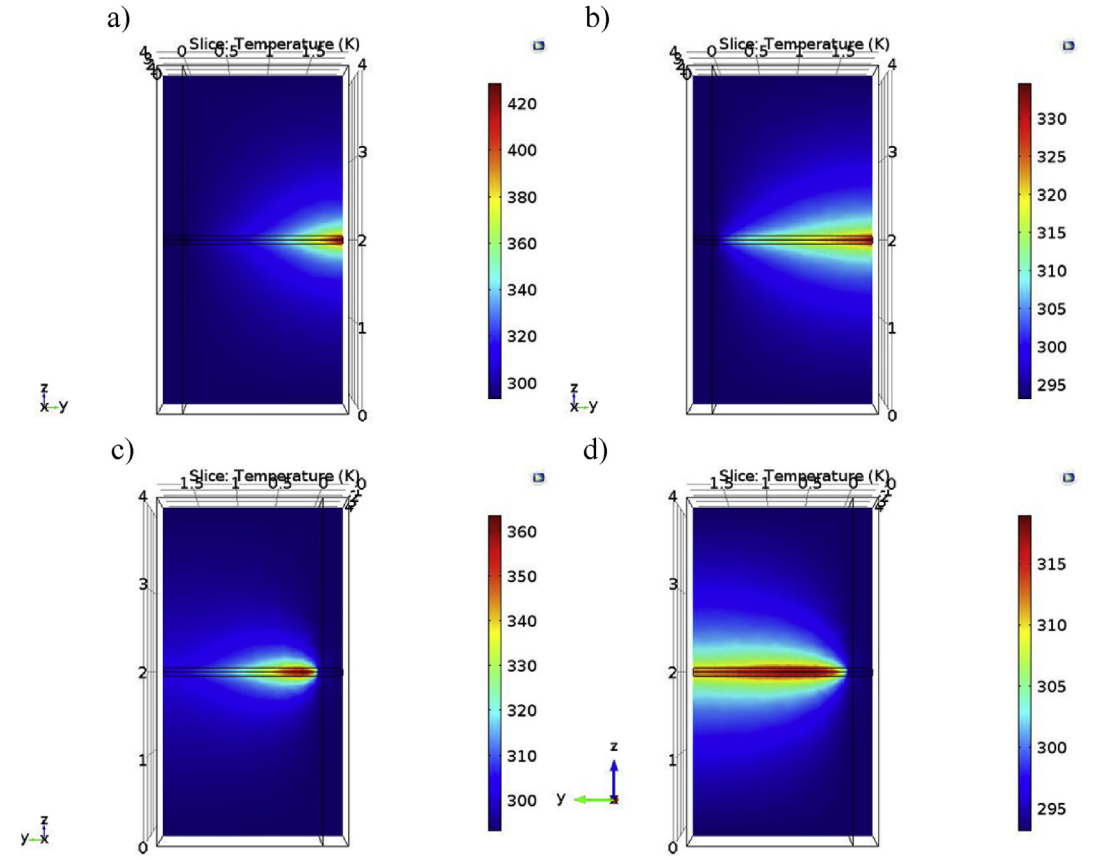

Fig. 3. Temperature distribution under 500 mW pump power: front pumping: a) 975 nm b) 940 nm; back pumping: c) 975 nm d) 940 nm.

are on the front face and the coating may be damaged.

On the other hand when the pump power is incident on the back side (the saturable absorber side) of the microchip; the highest temperatures are not registered at the end faces nor at the bonding face but deep inside the glass medium, these temperatures are lower than the previous case. The heat sink effect of the spinel crystal is strengthened in this case especially at 975 nm wavelength due to its proximity to the heat source distribution. The maximum temperature drops from 430 K to 362 K at 975 nm and from 335 K to 320 K at 940 nm. Comparing the temperature distributions in Fig. 3, one can see that in the case of back pumping at 940 nm the temperature distribution is larger and more homogenous than the rest of cases.

Using the solution of the heat equation, the Von Mises stresses and end faces deformations can be estimated taking into account the interaction between the glass and MALO crystal. Fig. 4 shows the Von Mises stress distribution and deformations for each case.

Beside its heat sink behavior, Co:MALO significantly decreases the deformation and bulge on the pumped face where the dichroic input mirror is coated. The situation is similar to the case of composite rod. The glass is subject to thermal deformation but the contact with MALO crystal, which does not absorb radiations and so is not heated considerably, generates a pressure and stress against this end face which decreases the deformation on this side. However such pressure will extend the rest of the bulge to the other side and raise the stresses on the bonding surface which should be always lower than the breakup stress threshold of the diffusion bonding. Fig. 5 shows the Von Mises stress of the bonding cross-section between glass and MALO crystal.

In the case of front pumping under 500 mW average power, the maximum stress was 3.5×10^6 N/m^2 at 975 nm and this is the lowest value among all configurations, whereas the deep penetration of the 940 nm radiations increases this value to 5.5×10^6 N/m^2.

On the other hand in case of the back pumping, the maximum stress increases at both wavelengths. The heated glass is subject of extension which is countered by the colder MALO crystal. The maximum stress increases to 2.6×10^7 N/m^2 and 9×10^6 N/m^2 at 975 nm and 940 nm respectively.

Analyzing these results, we can conclude that the safest configuration for the diffusion bounding is the front pumping at 975 nm whereas the most dangerous one is the back pumping at 975 nm.

Concerning the thermal lensing, a rigorous approach to estimate the thermal focal length was done by calculating the optical path difference on the axial propagation of the laser radiations. For a paraxial coherent beam the formula is derived as follows [21,22]:

$$OPD(r) = 2\int_0^L \left[\frac{dn_0}{dT} + (n_0 - 1)(1+\upsilon)\alpha_T + n_0^3\alpha_T C_r\right]\Delta T(r,y)dy \tag{3}$$

Where OPD(r) is the radial distribution of the thermally induced optical path difference (The other symbols are in table).

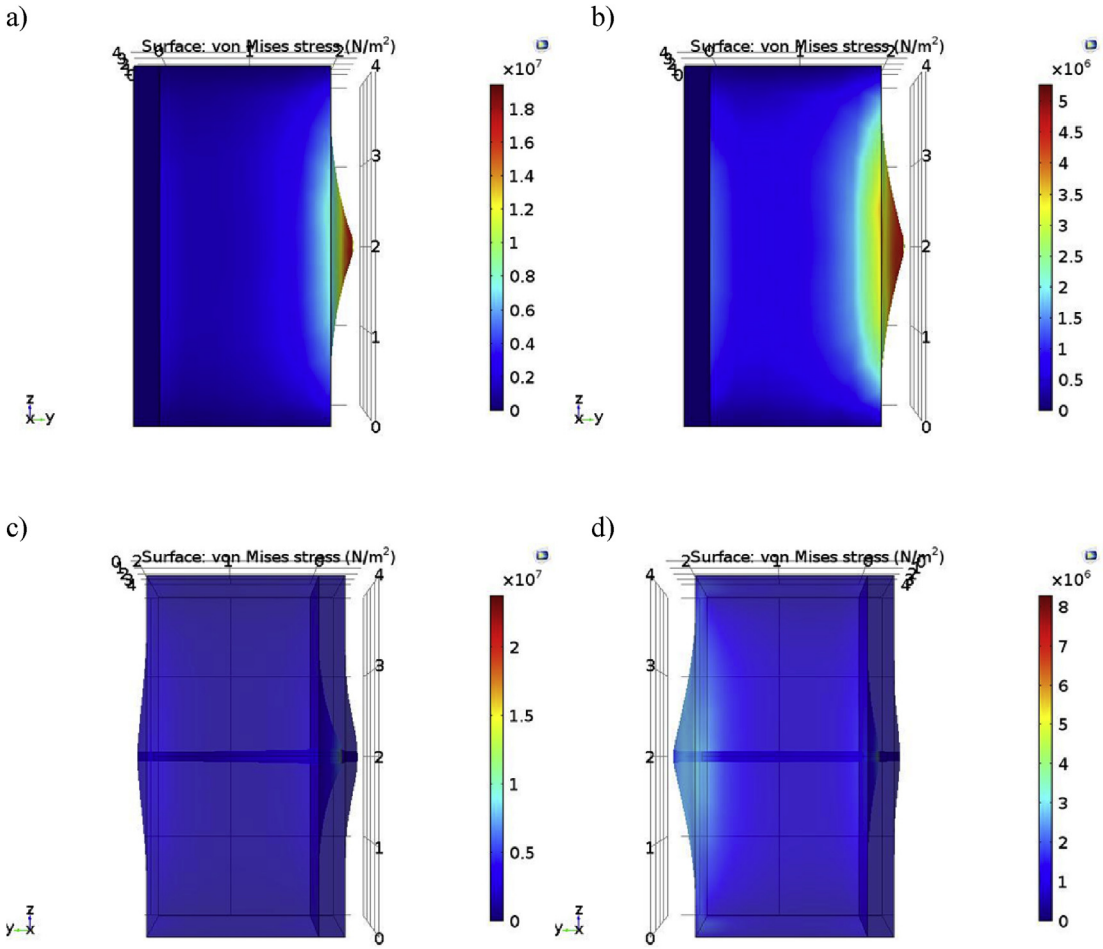

Fig. 4. Von Mises stress distribution and deformation under 500 mW pump power: front pumping: a) 975 nm b) 940 nm; back pumping: c) 975 nm d) 940 nm.

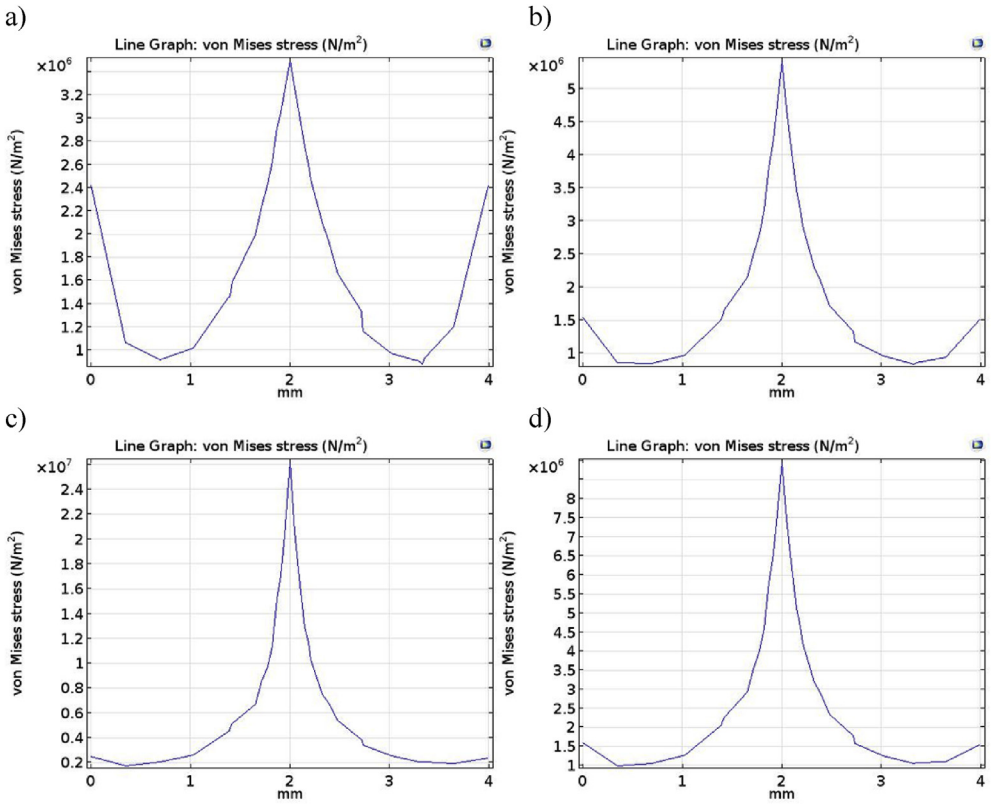

Fig. 5. Von Mises stress in the bonding area cross-section 500 mW pump power: front pumping: a) 975 nm b) 940 nm; back pumping: c) 975 nm d) 940 nm.

The first term is related to the change of the refractive index with temperature, the second term is related to the end face bulging and the third term is related to stress induced birefringence which is neglected in this case.

Despite of the negative thermo-optical coefficient of the phosphate glass, the plane parallel monolithic microchip laser is stabilized by the strong positive thermal lens induced by the end face bulging.

Applying the integral (3) on the studied microchip:

$$OPD(r) = 2\int_0^{L_g}\left[\frac{dn_{0g}}{dT} + (n_{0g}-1)(1+\upsilon)\alpha_{Tg}\right]\Delta T(r,y)dy + 2\int_{L_g}^{L_g+L_{MALO}}\left[\frac{dn_{0malo}}{dT} + (n_{0malo} - 1)(1+\upsilon)\alpha_{Tmalo}\right]\Delta T(r,y)dy \quad (4)$$

Note that both glass and MALO crystal are included in the calculation of the OPD. Using the numerical solution of the heat equation for different pumping case and pump power, the OPD is estimated.

To estimate the thermal focal length, the calculated radial distribution of the optical path difference is fitted to the one introduced by a spherical lens which is quadratically dependent on the radial coordinate r (eq. (5)), over the extent of the beam radius inside the resonator (neglecting the aberrations)

$$OPD(r) - OPD(0) = -\frac{r^2}{f_{th}} \quad (5)$$

Fig. 6 shows the estimation of the thermal focal length versus the average incident pump power for each of the studied cases. One can see that using 940 nm wavelength greatly reduced the thermal focal length. This is due to the uniform absorption of the pump radiation which yields a uniform temperature distribution in the active media; this decreases the maximum temperature and the end face deformation.

Comparing between the front and back face pumping for each wavelength, we can see that using the back pumping configuration slightly decreases the thermal focal length. This decrease is more apparent at lower pump power. This is also shown in Table 2, where we can see clearly that the maximum temperature is decreased when using the back side pumping thanks to the high thermal conductivity of the MALO.

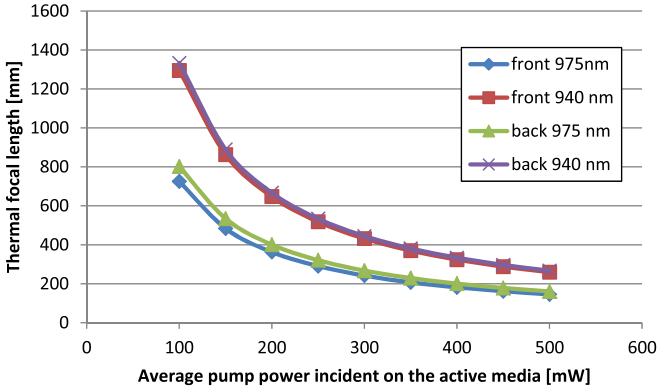

Fig. 6. Estimated thermal focal length versus the average pump power for different cases of pumping.

Table 2
Thermo-optical and mechanical results at 500 mW for different pumping cases.

Pump side	Front		Back	
Wavelength [nm]	975	940	975	940
Input mirror deformation [mm]	4×10^{-4}	1.5×10^{-4}	9.1×10^{-5}	4.2×10^{-5}
Output mirror deformation [mm]	2.9×10^{-5}	3×10^{-5}	7.7×10^{-5}	1×10^{-4}
Stress on bonding surface [N/m^2]	3.5×10^{6}	5.5×10^{6}	2.6×10^{7}	9×10^{6}
Maximum temperature [K]	428	334	363	319
Thermal focal length [mm]	145.07	259.04	160.31	266.71

4. Conclusion

Thermal analysis was performed for erbium-ytterbium phosphate glass diffusion bonded with Co MALO saturable absorber microchip laser. This analysis was based on the numerical solution of the heat equation taking into account the thermal and mechanical interactions between the glass and MALO crystal. The analysis was done for two pumping wavelengths 975 nm and 940 nm, and for two different sides of pumping front and back. It was shown that the back pumping configuration decreases the maximum temperature, end face bulging and thermal focal length due to the heat sink effect of MALO crystals, however it increases the stresses on the bonding area.

It was also shown that 940 nm back pumping configuration is the best configuration for reducing the thermal focal length and maximum temperature in the microchip laser, while the 975 nm front pumping is the safest configuration for the diffusion bonding.

Acknowledgement

The work was sponsored by the Polish National Centre for Research and Development. project DOB-1-6/1/PS/2014.

References

[1] G. Karlsson, V. Pasiskevicius, F. Laurell, J.A. Tellefsen, B. Denker, B.I. Galagan, V.V. Osiko, S. Sverchkov, Diode-pumped Er–Yb:glass laser passively Q switched by use of Co2+:MgAl2O4 as a saturable absorber, Appl. Opt. 39 (2000) 6188.
[2] S. Feng, W. Zhao-Hui, L. Shu-Jing, C. Hong, T. Jian-Guo, Z. Guang-Yin, B. Denker, S. Sverchkov, A passive q-switched microchip Er/Yb glass laser pumped by laser diode, Chin. Phys. Lett. 23 (2006) 1195.
[3] D. Nodop, J. Limpert, R. Hohmulth, W. Richter, M. Guina, A. Tunnermann, High-pulse-energy passively Q-switched quasi-monolithic microchip lasers operating in the sub-100-ps pulse regime, Opt. Lett. 32 (2007) 2115.
[4] P. Laporta, S. De Silvestri, V. Magni, O. Svelto, Diode-pumped cw bulk Er:Yb: glass laser, Opt. Lett. 16 (1991) 1952.
[5] J.A. Hutchinson, T.H. Allik, Diode array pumped Er, Yb: phosphate glass laser, Appl. Phys. Lett. 60 (1992) 1424.
[6] J. Mlynczak, K. Kopczynski, Z. Mierczyk, M. Malinowska, P. Osiwianski, Comparison of cw laser generation in Er3+,Yb3+:glass microchip lasers with different types of glasses, Opto-electro. Rev. 19 (2011) 87.
[7] S. Taccheo, G. Sorbello, P. Laporta, G. Karlsson, T. Laurell, 230-mW diode-pumped single-frequency Er:Yb laser at 1.5 μm, IEEE Photonics Technol.Lett. 13 (2001) 19.
[8] J. Mlynczak, K. Kopczynski, Z. Mierczyk, Generation investigation of eye-safe microchip lasers pumped by 974 nm and 939 nm wavelength, Opt. Appl. 38 (2008) 657–668.
[9] B. Denker, B. Galagan, V. Osiko, S. Sverchkov, Materials and components for miniature diode–pumped 1.5–μm erbiglass lasers, Laser Phys. 12 (2002) 697.
[10] J. Mlynczak, K. Kopczynski, Z. Mierczyk, M. Malinowska, P. Osiwianski, Pulse generation at 1.5 μm wavelength in new EAT14 glasses doped with Er3+ and Yb3+ ions, Opto-electro. Rev. 20 (2012) 14.
[11] J. Mlynczak, N. Belghachem, Monolithic thermallybondedEr3+, Yb^{3+}:glass/Co^{2+}:$MgAl_2O_4$ microchip lasers, Opt. Commun. 356 (2015) 166–169.
[12] L.I. Burov, L.G. Krylova, Optimization of Yb-Er microchip laser parameters, J. Appl. Spec. 79 (2012) 376.
[13] J. Degnan, Optimization of passively q-switched lasers, J. Quant. Electron 31 (1995) 1890–1901.
[14] J. Mlynczak, K. Kopczynski, Z. Mierczyk, Optimization of passively repetitively q-switched three-level lasers, IEEE J. Quantum Electron 44 (2008) 1152–1157.
[15] N. Belghachem, J. Mlynczak, Numerical simulation and optimization of passively q-switched erbium microchip lasers, Laser Phys. 25 (2015).
[16] J. MSerres, X. Mateos, P. Loiko, K. Yumashev, N. Kuleshov, V. Petrov, U. Griebner, M. Aguilo, F. Diaz, Diode-pumped microchip Tm:KLu(WO_4)$_2$ laser with mode than 3 W of output power, Opt. Lett. 39 (2014).
[17] F. Song, S. Liu, Z. Wu, H. Cai, X. Zhang, L. Teng, J. Tian, Determination of the thermal loading in diode-pumped erbium-ytterbium-codoped phosphate glass microchip laser, J. Opt. 24 (9) (2007).
[18] S. Liu, F. Song, H. Cai, T. Li, B. Tian, Z. Wu, J. Tian, Effect of the thermal lens on beam quality and mode matching in LD pumped Er-Yb-codoped phosphate glass microchip laser, J. Phys. D Appl. Phys. 41 (2008).
[19] M. Kerobyan, R. Konstanyan, V. Nersesyan, S. Soghomonyan, Thermal lensing in diode pumped Nd3+:YVO4/LiNbO3 green microchip laser, J. Phys.:Conf. Ser. 541 (2014).
[20] S.C. Tidwell, J.F. Seamans, M.S. Bowers, A.K. Cousins, Scaling CW diode-end-pumped Nd:YAG lasers to high average powers (Integ OPD), IEEE J. Quantum Electron 28 (1992) 997–1009.
[21] S. Wang, H.J. Eichler, X. Wang, F. Kallmeyer, J. Ge, T. Riesbeck, J. Chen, Diode end pumped Nd:YAG at 946nm with high pulse energy limited by thermal lensing, Appl. Phys. B 95 (2009) 721–730.
[22] G. Li, B.Q. Yao, X.M. Duan, C.H. Zhang, Y.Z. Wang, Thermal analysis and laser performance modeling of a dual-end pumped c-cut CW Tm:YAP laser, J. Phys. B 43 (2010).